Inorganic Chemistry

Article

pubs.acs.org/IC

Synthesis of a Uranyl Persulfide Complex and Quantum Chemical Studies of Formation and Topologies of Hypothetical Uranyl Persulfide Cage Clusters

Daniel J. Grant,[†] Zhehui Weng,[‡] Laurent J. Jouffret,[‡] Peter C. Burns,*[,‡,§] and Laura Gagliardi*[,†]

[†]Department of Chemistry, University of Minnesota and Supercomputing Institute, 207 Pleasant Street Southeast, Minneapolis, Minnesota 55455, United States

[‡]Department of Civil Engineering and Geological Sciences and [§]Department of Chemistry and Biochemistry, University of Notre Dame, Notre Dame, Indiana 46556, United States

Supporting Information

ABSTRACT: The compound $Na_4[(UO_2)(S_2)_3](CH_3OH)_8$ was synthesized at room temperature in an oxygen-free environment. It contains a rare example of the $[(UO_2)(S_2)_3]^{4-}$ complex in which a uranyl ion is coordinated by three bidentate persulfide groups. We examined the possible linkage of these units to form nanoscale cage clusters analogous to those formed from uranyl peroxide polyhedra. Quantum chemical calculations at the density functional and multiconfigurational wave function levels show that the uranyl–persulfide–uranyl, U–(S_2)–U, dihedral angles of model clusters are bent due to partial covalent interactions. We propose that this bent interaction will favor assembly of uranyl ions through persulfide bridges into curved structures, potentially similar to the family of nanoscale cage clusters built from uranyl peroxide polyhedra. However, the U–(S_2)–U dihedral angles predicted for several model structures may be too tight for them to self-assemble into cage clusters with fullerene topologies in the absence of other uranyl-ion bridges that adopt a flatter configuration. Assembly of species such as $[(UO_2)(S_2)(SH)_4]^{4-}$ or $[(UO_2)(S_2)(C_2O_4)_4]^{4-}$ into fullerene topologies with ~60 vertices may be favored by use of large counterions.

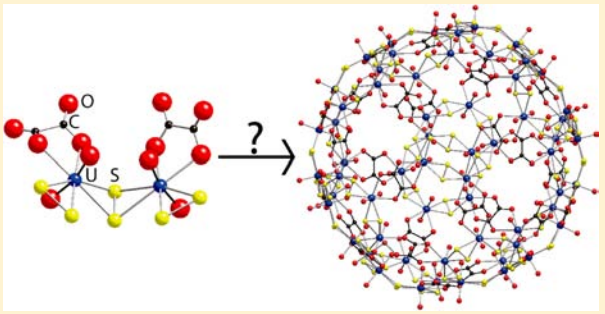

1. INTRODUCTION

Nanoscale cage clusters based on transition metals and oxygen have been extensively studied owing to their structural diversity and broad applications.[1−6] Despite potential applications in an advanced nuclear energy system, studies of metal oxide clusters have only relatively recently been extended into the actinide series. Given the range of oxidation states and coordination polyhedra accessible in the early actinides,[7] it is reasonable to expect that actinide oxide cluster complexity will rival that of transition metal oxides. Self-assembly of U(IV), U(V), and Pu(IV) oxide clusters has been reported.[8−13] We reported that more than 30 nanoscale clusters built from as many as 120 uranyl peroxide polyhedra self-assemble in aqueous solution under ambient conditions.[14−27] Potential applications of these clusters in nuclear energy as well as their importance in environmental transport of actinides stimulated our interest. For example, uranyl peroxide clusters may form where damaged nuclear fuel interacts with water, and such clusters may persist in the environment.[28,29]

We are interested in developing clusters built from uranyl ions that have a broad range of topologies, sizes, chemical compositions, and properties. Such clusters may have applications in nuclear material recycling and as precursors for the synthesis of new types of actinide materials. To date, most of the clusters we have reported are cages of uranyl hexagonal bipyramids that are three connected to other hexagonal bipyramids by sharing equatorial edges between them. The resulting topologies are complex and include several fullerenes as well as clusters that have topological squares. All of the uranyl ions in these clusters are coordinated by bidentate peroxide groups that form equatorial edges of the corresponding uranyl hexagonal bipyramids and bridge uranyl ions. On the basis of both experimental and computational studies, it appears that bonding interactions between the uranyl ions and the peroxide groups favor a bent U–(O_2)–U dihedral angle, which in turn encourages the topological curvature essential for cage cluster formation.[16,30,31]

We seek to extend the family of uranyl-based cage clusters using bridges other than peroxide. Central to this goal is finding ways to bridge uranyl ions that foster curved structures, so as to form nanoscale materials rather than extended structures. Accordingly, we hypothesize that bidentate persulfide bridges between uranyl ions may favor self-assembly of uranyl persulfide polyhedra into cage clusters in an analogous fashion to the peroxide ligands. However, hexavalent uranium, which

Received: April 26, 2012
Published: July 5, 2012

   dx.doi.org/10.1021/ic3008574 | *Inorg. Chem.* 2012, 51, 7801−7809

exists as the linear $(UO_2)^{2+}$ dioxo uranyl ion, is highly oxophyllic. Synthesis of our target complexes, which involve coordination of uranyl ions with bidentate persulfide ligands, requires exclusion of O_2 from reaction conditions. The basic building unit for our proposed cage clusters is a uranyl polyhedron with at least one bidentate persulfide ligand. The $[(UO_2)(S_2)_3]^{4-}$ species has been reported in compounds $Cs_4(UO_2)(S_2)_3$ and $Na_4(UO_2)(S_2)_3{\cdot}Na_2S_3$, which were synthesized from molten alkali metal polysulfide salts at elevated temperatures.[32] Compound $[(n\text{-}C_3H_7)_2NH_2^+]_2[UO_2((n\text{-}C_3H_7)_2NCOS)_2(S_2)]^{2-}$ was also reported.[33]

Here we present a synthetic route for $[(UO_2)(S_2)_3]^{4-}$ and compound $Na_4[(UO_2)(S_2)_3](CH_3OH)_8$ at room temperature in a controlled atmosphere and characterization of its crystal structure. Extending our experimental study beyond this compound will require an appropriate solvent and a judicious selection of counterions and other experimental conditions. We have therefore undertaken a computational study of hypothetical complexes that contain persulfide bridges between uranyl ions to probe the feasability of assembling such units into uranyl persulfide cage clusters and provide guidance for selection of synthesis conditions.

2. EXPERIMENTAL SECTION

2.1. Synthesis of $Na_4[(UO_2)(S_2)_3](CH_3OH)_8$. *Caution: Although isotopically depleted uranium was used in these reactions, it is toxic and radioactive and should only be handled by properly trained personel using appropriate facilities.* All chemicals were obtained from commercial sources and used as received. Uranyl triflate $(UO_2(CF_3SO_3)_2)$ was synthesized by reacting UO_3 and triflic acid using established methods.[34] The uranyl persulfide complex was synthesized in an inert atmosphere glovebox using Schlenk techniques. Synthesis of $Na_4[(UO_2)(S_2)_3](CH_3OH)_8$ was achieved using multiple methods. The general procedure was to react Na_2S and S in an appropriate solvent to produce polysulfides and enhance the yield of polysulfides using basic conditions. As the triflate complexes uranyl only weakly, we expected persulfide to bind to uranyl and give the desired complex. We synthesized the target complex, $[(UO_2)(S_2)_3]^{4-}$, using either methanol or ethanol as solvent, as shown by crystal-structure analyses of the resulting compounds. Experiments were conducted using LiOH, NaOH, and KOH, but only those with NaOH gave crystals. Synthesis without a base failed to yield crystals, possibly because insufficient persulfide was produced.

The crystal used for structure characterization was synthesized by adding 10 mL of methanol as solvent to a Schlenk flask containing Na_2S (0.0781 g, 1 mmol), S (0.0481 g, 1.5 mmol), NaOH (0.08 g, 2 mmol), and $UO_2(CF_3SO_3)_2$ (0.0293 g, 0.05 mmol). The reaction mixture was stirred for 4 h and was then filtered. Brown-black needle-like crystals were obtained via slow diffusion of the filtrate into air. Crystals of the same compound where obtained by placing 10 mL of methanol in a Schlenk flask that contained Na_2S (0.0781 g, 1 mmol), S (0.0481 g, 1.5 mmol), NaOH (0.04 g, 1 mmol), and $UO_2(CF_3SO_3)_2$ (0.0568 g, 0.1 mmol). The solution was then stirred for 4 h and filtered. Black-brown needle-like crystals grew during slow diffusion of toluene into the filtrate.

Both synthesis methods described in the previous paragraph produced $Na_4[(UO_2)(S_2)_3](CH_3OH)_8$ crystals in a yield of ~20% on the basis of uranium and have been repeated. Black-brown acicular crystals of $Na_4[(UO_2)(S_2)_3](CH_3OH)_8$ as much as 5 mm in length form in the absence of other precipitates (Supporting Information).

2.2. Characterization of $Na_4[(UO_2)(S_2)_3](CH_3OH)_8$. Brown-black crystals of $Na_4[(UO_2)(S_2)_3](CH_3OH)_8$ change color and decompose after brief exposure to air, making characterization challenging.

A suitable crystal was selected using a polarized-light microscope, placed in oil on a cryoloop, and cooled to 110 K in a stream of N_2 for X-ray diffraction studies. It was necessary to avoid contacting the compound with air, which was achieved by injecting mother solution containing crystals directly into the oil. Placement of the crystal, enclosed in a droplet of oil, into the N_2 gas stream permitted collection of diffraction data. Data were collected using a Bruker APEX II detector mounted on a three-circle goniometer equipped with Mo Kα radiation provided by a conventional tube. Data were integrated and corrected for background, polarization, and Lorentz effects using the computer program APEX II.[35] An empirical correction for absorption was done with SADABS.

Solution of the structure of $Na_4[(UO_2)(S_2)_3](CH_3OH)_8$ was done in space group *P*-1. Solution and refinement of the structure was straightforward using the SHELXTL[36] suite of software. The positions of the U atoms were obtained from a direct-methods solution, and the structure model was constructed by identifying atoms in subsequent difference-Fourier maps that were calculated following least-squares refinement of the partial-structure models. The final cycles of refinement included all atomic positional parameters, anisotropic displacement parameters for the U and S atoms, and isotopic displacement parameters for the Na, O, and C atoms. H atoms of OCH_3 were excluded from refinement, as it is difficult to identify H atoms in a compound containing U, which dominates X-ray scattering. Crystallographic information is summarized in Table 1, and selected interatomic distances are provided in Table 2.

Table 1. Crystallographic Parameters for $Na_4[(UO_2)(S_2)_3](CH_3OH)_8$

cryst syst	triclinic
space group	*P*-1
wavelength	0.71073 Å
lattice params	a = 10.862(2) Å
	b = 11.039(2) Å
	c = 13.633(2) Å
	α = 83.681(2)°
	β = 67.292(1)°
	γ = 67.300(2)°
number of formula units	Z = 2
calcd density (D_x)	3.841 g/cm^3
$2\theta_{max}$	57.0°
$F(000)$	1552
abs coefft μ	12.78 mm^{-1}
measd reflns	10 158
unique reflns	4235
R_{int}/R_σ	0.0368/0.0724
reflns with $\lvert F_o\rvert \geq 4\sigma(F_o)$	3698
R_1/R_1 with $\lvert F_o\rvert \geq 4\sigma(F_o)$	0.0362/0.0278
wR_2/goodness of fit (S)	0.0618/0.95

A UV−vis spectrum was collected for a single crystal of $Na_4[(UO_2)(S_2)_3](CH_3OH)_8$ using a Craic Technologies microspectrophotometer. The crystal was placed on a quartz slide under mineral oil, and data were collected from 200 to 1600 nm. An infrared spectrum was likewise collected using a SenSIR spectrometer and a diamond total attenuated reflectance (ATR) objective. Spectra are provided in the Supporting Information.

Raman spectra were collected for a single crystal of $Na_4[(UO_2)(S_2)_3](CH_3OH)_8$ to confirm the presence of persulfide (Supporting Information) using a Bruker Sentinel system linked via fiber optics to a video-assisted Raman probe in a microscope mount. The laser wavelength was 785 nm with a power of 400 mW. The instrument is equipped with a high-sensitivity, TE-cooled 1024 × 255 CCD array. Spectra were collected for 5 s with 3 signal accumulations in the range from 80 to 3200 cm^{-1}. As crystals of $Na_4[(UO_2)(S_2)_3](CH_3OH)_8$ are unstable in air, spectra were collected at time increments of a few seconds until the crystals decomposed over the course of a few minutes.

2.3. Computational Methods. Quantum chemical calculations were performed using density functional theory (DFT)[37,38] and

dx.doi.org/10.1021/ic3008574 | Inorg. Chem. 2012, 51, 7801−7809

Table 2. Selected Bond Lengths (Angstroms) for $Na_4[(UO_2)(S_2)_3](CH_3OH)_8$.

U(1)−O(1)	1.852(3)	Na(1)−O(9)	2.324(5)
U(1)−O(2)	1.858(3)	Na(1)−O(7)	2.337(4)
U(1)−S(1)	2.751(1)	Na(1)−O(6)	2.352(5)
U(1)−S(2)	2.768(1)	Na(1)−O(2)	2.553(4)
U(1)−S(3)	2.784(2)	Na(1)−S(1)	2.953(3)
U(1)−S(4)	2.796(2)	Na(1)−S(3)	3.043(3)
U(1)−S(5)	2.785(2)	Na(2)−O(8)	2.329(5)
U(1)−S(6)	2.788(2)	Na(2)−O(6)	2.394(5)
S(1)−S(5)	2.082(2)	Na(2)−O(7)	2.399(4)
S(2)−S(4)	2.081(2)	Na(2)−O(2)	2.423(4)
S(3)−S(6)	2.077(2)	Na(2)−O(2)	2.534(5)
C(1)−O(9)	1.465(9)	Na(2)−S(5)	2.912(2)
C(2)−O(10)	1.412(9)	Na(3)−O(3)	2.330(5)
C(3)−O(4)	1.449(7)	Na(3)−O(4)	2.398(5)
C(4)−O(7)	1.428(8)	Na(3)−O(5)	2.414(5)
C(5)−O(8)	1.422(8)	Na(3)−O(1)	2.416(4)
C(6)−O(6)	1.452(7)	Na(3)−O(1)	2.540(4)
C(7)−O(3)	1.428(8)	Na(3)−S(4)	2.868(2)
C(8)−O(5)	1.455(8)	Na(4)−O(10)	2.296(5)
		Na(4)−O(5)	2.330(4)
		Na(4)−O(4)	2.381(4)
		Na(4)−O(1)	2.545(4)
		Na(4)−S(6)	2.975(3)
		Na(4)−S(2)	3.007(2)

multiconfigurational methods (CASSCF/CASPT2)[39,40] for the hypothetical clusters $[(UO_2)_2(S_2)(O_2)_4]^{6-}$, $[(UO_2)(SH)(O_2)_2]_2^{6-}$, $[(UO_2)_2(S_2)(C_2O_4)_4]^{6-}$, $[(UO_2)_2(SH)_2(C_2O_4)_4]^{6-}$, and $[(UO_2)(S_2)(C_2O_4)]_5^{10-}$, including counterions in most cases. Model clusters were chosen to facilitate comparison of persulfide-bridged uranyl cluster geometries with those containing peroxide bridges studied previously.[31] Initial structures were derived from previously studied peroxide clusters by replacing peroxide and hydroxyl groups shared between uranyl ions with persulfide and sulfhydryl groups, respectively. The counterions Li, Na, K, Rb, and Cs were randomly distributed about the starting structure, and geometry optimizations were performed without symmetry constraints. We also optimized the geometry of a cluster with composition $Na[(UO_2)(S_2)_3]$ for comparison to our experimentally determined structure. Vibrational harmonic frequencies verified the optimized structures as local minima.

Geometry optimizations were performed at the DFT level employing the resolution of identity (RI)[41] approximation, Perdew−Burke−Ernzerhof (PBE) exchange-correlation functional,[42] triple-ζ valence plus polarization (def-TZVP)[43,44] basis set, and corresponding auxiliary RI basis set on all atoms.[41] Quasi-relativistic pseudopotentials were used for U with 60 core electrons.[44,45] Each cluster was reoptimized within the conductor-like solvation model (COSMO)[46] implementation to estimate solvent effects. The RI-PBE/def-TZVP (COSMO) method has reproduced experimental parameters in actinide-containing systems.[31,47] All DFT optimizations and frequency calculations were performed with the TURBOMOLE 5.10 program package.[43,48]

Energy decomposition analysis (EDA) was performed at the PBE/TZ2P level with small core pseudopotentials and scalar relativistic effects from the ZORA formalism.[49] EDA was performed using the ADF program[50] based on the methods of Morokuma[51,52] and Ziegler.[53−55] The bond energy ΔE_{BDE} is the summation of the energy change required to deform the structure of the free fragment to that in the molecule, $\Delta E_{preperation}$, and the instaneous interaction energy between fragments. $\Delta E_{interaction}$ is further subdivided into the summation of three components: ΔE_{elstat}, classical Coulomb interaction; ΔE_{Pauli}, exchange repulsion; and ΔE_{orb}, orbital interaction between the occupied and the virtual orbitals of the fragments indicating covalent bonding. The electrostatic interaction, ΔE_{elstat}, and orbital energies, ΔE_{orb}, are typically attractive, while the Pauli repulsion, ΔE_{Pauli}, is replusive.

Single-point multiconfigurational complete active space (CASSCF)[56] and second-order perturbation theory (CASPT2)[41] calculations were performed at the DFT-optimized geometries. Scalar relativistic effects were included using the Douglas−Kroll−Hess[57] Hamiltonian and the relativistic all electron ANO-RCC basis sets with double-ζ quality (ANO-RCC-VDZP)[56] with the contractions: U [8s7p5d3f1g], C and O [3s2p1d], and H [1s]. All systems are single configurational. An ideal active space for diuranyl clusters is 24 electrons in 24 orbitals.[58,59] However, such a calculation is computationally unfeasible, and the final active space includes the four highest occupied molecular orbitals (HOMO) and four lowest unoccupied molecular orbitals (LUMO), giving eight electrons in eight orbitals. Six orbitals are bonding or antibonding uranyl peroxo orbitals, and the remaining are $U-S_{persulfide}$ orbitals. For the pentauranyl clusters, CASSCF/CASPT2 calculations were not performed as five uranium atoms are prohibitively large to treat with this method.

CASSCF/CASPT2 calculations were performed with the MOLCAS 7.3 package.[60] Computational costs arising from the two-electron integrals were reduced by employing the Cholesky decomposition technique in all CASSCF/CASPT2 calculations[61−63] combined with the local exchange screening.[64] The CASSCF/CASPT2 approach has been successfully applied in studying many actinide-containing systems[31,65−69] and employed to the uranyl persulfide clusters.

3. RESULTS

3.1. Structure of $Na_4[(UO_2)(S_2)_3](CH_3OH)_8$. Reaction of $UO_2(CF_3SO_3)_2$ with NaS_2, S, and NaOH contained within methanol or ethanol at room temperature results in formation of the $[(UO_2)(S_2)_3]^{4-}$ species, which was crystallized to give the compound $Na_4[(UO_2)(S_2)_3](CH_3OH)_8$. Previously, the $[(UO_2)(S_2)_3]^{4-}$ species was obtained in molten alkali metal polysulfide salts at 350−400 °C. Development of a synthesis method for the $[(UO_2)(S_2)_3]^{4-}$ species at room temperature is essential to our planned attempts to create cage clusters based upon this species.

The structure of $Na_4[(UO_2)(S_2)_3](CH_3OH)_8$, which crystallizes in space group *P*-1, contains one symmetrically distinct U(VI) cation (Figure 1). It is present as an approximately linear uranyl ion with bond lengths of 1.852(3) and 1.858(3) Å. The uranyl dioxo cation is coordinated by three bidentate persulfide groups, as confirmed from Raman spectroscopic studies, such that the $(S_2)^{2-}$ groups are located along equatorial edges of the uranyl hexagonal bipyramid. The U−S bond lengths range from 2.751(1) to 2.796(1) Å, and the S−S bond lengths range from 2.077(2) to 2.082(2) Å.

The uranyl ion bond lengths in $Na_4[(UO_2)(S_2)_3](CH_3OH)_8$ are elongated relative to those in structures where uranyl ions are coordinated by O atoms of various oxy anions, where the average is 1.78(3) Å.[70] Only three previously reported structures contain U^{6+} uranyl ions coordinated by bidentate persulfide ions. In $Cs_4(UO_2)(S_2)_3$ and $Na_4(UO_2)(S_2)_3{\cdot}Na_2S_3$, which contain the same uranyl persulfide unit as $Na_4[(UO_2)(S_2)_3](CH_3OH)_8$, the uranyl ion U−O bond lengths range from 1.79(2) to 1.86(2) Å and from 1.84(2) to 1.86(2) Å, respectively.[32] In $[(n\text{-}C_3H_7)_2NH_2^+]_2[UO_2((n\text{-}C_3H_7)_2NCOS)_2(S_2)]^{2-}$, the uranyl ion is coordinated by one bidentate persulfide ligand and the $U-O_{Ur}$ bond length is 1.815(6) Å.[33] Electroneutrality in $Na_4[(UO_2)(S_2)_3](CH_3OH)_8$ requires that the U cation be hexavalent, which is consistent with the UV−vis spectrum that demonstrates the presence of persulfide (Supporting Information).

dx.doi.org/10.1021/ic3008574 | Inorg. Chem. 2012, 51, 7801−7809

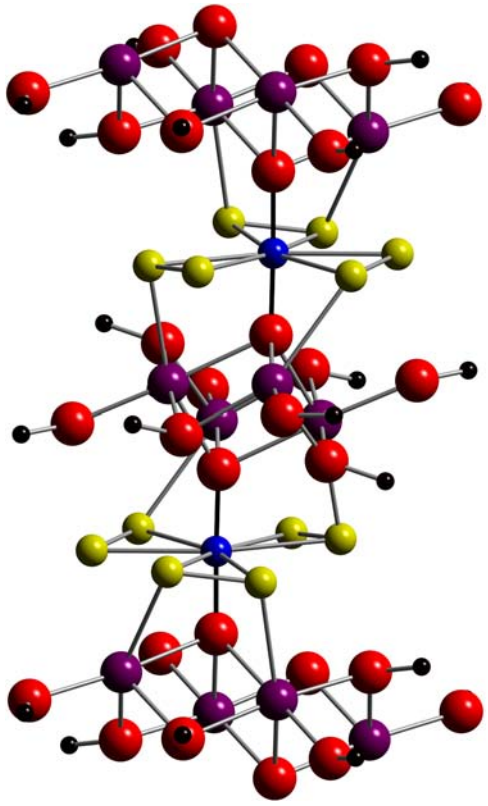

Figure 1. Ball-and-stick representation of the structure of $Na_4[(UO_2)(S_2)_3](CH_3OH)_8$. U, O, S, C, and Na atoms are shown as blue, red, yellow, black, and purple spheres, respectively. U−O bonds within the uranyl ion are shown by black lines; all others are shown as gray cylinders.

The S atoms of the three persulfide groups of the U(1) coordination polyhedron are not perfectly coplanar. Rather, they are in the range from 0.004 to 0.143 Å from the best-fit plane through them that also passes through the central U atom.

Each O atom of the U(1) uranyl ion is bonded to three Na cations, with Na−O bond lengths ranging from 2.416(4) to 2.553(4) Å. The Na cations are also coordinated by methanol groups, resulting in heteropolyhedral chains (Figure 1). The Na cations are further coordinated by one or two S ions at distances in the range from 2.868(2) to 3.043(3) Å.

The infrared spectrum (Supporting Information) collected for $Na_4[(UO_2)(S_2)_3](CH_3OH)_8$ contains modes that are readily assignable to uranyl stretches (820 cm^{-1})[71] and methanol. The Raman spectra (Supporting Information) demonstrate the presence of persulfide units in $Na_4[(UO_2)(S_2)_3](CH_3OH)_8$ with vibrations at 466 and 478 cm^{-1} [72,73] and that the persulfide breaks down over the course of less than 10 min when exposed to air.

3.2. Computational Results. Clusters $[(UO_2)_2(S_2)(O_2)_4]^{6-}$, $[(UO_2)_2(SH)_2(O_2)_4]_2^{6-}$, $[(UO_2)_2(S_2)(C_2O_4)_4]^{6-}$, $[(UO_2)(SH)(C_2O_4)_2]_2^{6-}$, and $[(UO_2)_5(S_2)_5(C_2O_4)_5]^{10-}$ were considered, both with a negative charge and with counterions added to give an overall molecular charge of zero. Selected geometry parameters are reported in Tables 3−7. The optimized molecular structures of exemplary clusters are illustrated in Figures 2 and 3. Details of the remainder are in the Supporting Information. The bonding molecular orbitals in $Na_6[(UO_2)_2(S_2)(O_2)_4]$ and $Na_6[(UO_2)_2(SH)_2(O_2)_4]$ are depicted in Figures 4 and 5, respectively, and others are detailed in the Supporting Information. The U−(S_2)−U persulfide and U−(O_2)−U peroxide dihedral angles of the diuranyl and pentauranyl clusters are shown as a function of the ionic radius of the counterion in Figures 6 and 7, respectively.

Optimization of bare $[(UO_2)_2(S_2)(O_2)_4]^{6-}$ gave a structure with a bent U−(S_2)−U dihedral angle, but small imaginary frequencies indicate it was not a true minimum. A true minimum was only obtained upon inclusion of counterions to give a molecular charge of zero. A potential energy scan of the U−(S_2)−U dihedral angle of the bare $[(UO_2)_2(S_2)(O_2)_4]^{6-}$ cluster indicated a rather flat surface where the energy difference between the bent and the fully planar (U−(S_2)−U dihedral angle = 180°) structures was a mere 3 kcal/mol. Without the presence of counterions, the U−(S_2)−U dihedral angle is very pliable and there is no significant energetic penalty to deform to the flat structure. The counterions assist in maintaining the bent U−(S_2)−U dihedral angle dominantly through interactions with the uranyl ion oxygen atoms. The importance of counterions was also demonstrated in the analogous $[(UO_2)_2(O_2)_5]^{6-}$ cluster, which initially optimized to a 180° U−(O_2)−U dihedral angle. Only after inserting six Na ions was a bent 144° angle obtained. No experimental structure is available for $Na_6[(UO_2)_2(S_2)(O_2)_4]$, but the U−$(S_2)$−U dihedral angle is 18° more bent than the computed U−(O_2)−U dihedral angle in an analogous structure.[31]

Geometry optimization of $Na_6[(UO_2)_2(SH)_2(O_2)_4]$ results in a U−$(SH)_2$−U dihedral angle of 178°, which is approximately equivalent to the analogous U−$(OH)_2$−U angle of the diuranyl peroxide cluster.[31] $Na_6[(UO_2)_2(S_2)(C_2O_4)_4]$, with bidentate oxalate groups, optimizes to a U−(S_2)−U dihedral angle of 108°, which is 17° and 24° smaller than the equivalent angle in $Na_6[(UO_2)_2(S_2)(O_2)_4]$ and the analogous peroxide cluster.[31] The geometry of $Na_6[(UO_2)_2(SH)_2(C_2O_4)_4]$ optimized to a U−$(SH)_2$−U dihedral angle of 164°, in contrast to the ∼180° dihedral angles found in the corresponding $Na_6[(UO_2)_2(SH)_2(O_2)_4]$ and peroxide clusters.[31]

$Na_{10}[(UO_2)_5(S_2)_5(C_2O_4)_5]$ contains five uranyl ions bridged by persulfide groups to form a pentagonal ring (Figure 3), with optimized U−(S_2)−U dihedral angles in the range of 117−

Table 3. Selected Geometry Parameters of $A_6[(UO_2)_2(S_2)(O_2)_4]$ (A = Li, Na, K, Rb, Cs) at the PBE/def-TZVP (COSMO) level[a]

A	$r(U-O)_U$	$r(U-S)_{per}$	$r(S-S)_{per}$	$r(U-U)_U$	$r(O-O)_{U-U}$	$\angle(OUO)_U$	∠USSU
Li	1.89−1.93	2.91−2.92	2.13	4.92	2.96−6.82	179.0−179.6	130.5
Na	1.89−1.92	2.93−2.94	2.13	4.88	3.14−6.71	177.4−178.2	125.5
K	1.89−1.91	2.96−3.00	2.13	4.90	3.16−6.57	178.0−178.2	123.6
Rb	1.89−1.90	2.97−3.00	2.13	4.94	3.27−6.53	177.7−178.6	125.1
Cs	1.89−1.90	2.98−3.00	2.13	4.99	3.39−6.47	177.1−178.3	126.5

[a]Range represents the shortest and longest, respectively. Notations: U = uranyl; per = persulfide. Distances in Angstroms and angles in degrees

dx.doi.org/10.1021/ic3008574 | Inorg. Chem. 2012, 51, 7801−7809

Table 4. Selected Geometry Parameters of $A_6[(UO_2)_2(SH)_2(O_2)_4]$ (A = Li, Na, K, Rb, Cs) at the PBE/def-TZVP (COSMO) Level[a]

A	$r(U-O)_U$	$r(U-S)_{sulf}$	$r(S-S)_{sulf}$	$r(U-U)_U$	$r(O-O)_{U-U}$	$\angle(OUO)_U$	∠USSU
Li	1.92	2.91	3.03	4.98	4.60	168.9	180.0
Na	1.91−1.92	2.94−3.00	3.27	4.97	4.65−4.73	170.5−171.9	178.3
K	1.90−1.91	3.05−3.08	3.16	5.25	5.08−5.09	174.4−175.1	178.0
Rb	1.90	3.06−3.08	3.19	5.25	5.11	175.6−175.9	178.2
Cs	1.90	3.08−3.09	3.53	5.06	4.81−4.94	174.0−174.5	178.3

[a]Range represents the shortest and longest, respectively. Notations: U = uranyl; sulf = sulfhydryl. Distances in Angstroms and angles in degrees

Table 5. Selected Geometry Parameters of $A_6[(UO_2)_2(S_2)(C_2O_4)_4]$ (A = Li, Na, K, Rb, Cs) at the PBE/def-TZVP (COSMO) Level[a]

A	$r(U-O)_U$	$r(U-S)_{per}$	$r(S-S)_{per}$	$r(U-U)_U$	$r(O-O)_{U-U}$	$\angle(OUO)_U$	∠USSU
Li	1.81−1.84	2.81−2.95	2.06	4.04	2.68−6.24	159.7−172.2	97.3
Na	1.81−1.83	2.88−2.90	2.06	4.37	2.96−6.29	169.6−173.0	108.3
K	1.81−1.83	2.90−2.91	2.06	4.61	3.14−6.38	174.8−175.2	116.2
Rb	1.81−1.83	2.91−2.92	2.06	4.69	3.18−6.43	176.0−176.2	118.5
Cs	1.82−1.83	2.91−1.92	2.06	4.76	3.22−6.47	176.8−177.5	121.2

[a]Range represents the shortest and longest, respectively. Notations: U = uranyl; per = persulfide. Distances in Angstroms and angles in degrees

Table 6. Selected Geometry Parameters of $A_6[(UO_2)_2(SH)_2(C_2O_4)_4]$ (A = Li, Na, K, Rb, Cs) at the PBE/def-TZVP (COSMO) Level[a]

A	$r(U-O)_U$	$r(U-S)_{sulf}$	$r(S-S)_{sulf}$	$r(U-U)_U$	$r(O-O)_{U-U}$	$\angle(OUO)_U$	∠USSU
Li	1.84−1.84	2.97−3.01	2.80	5.00	5.77−5.78	154.0−154.8	141.8
Na	1.85−1.85	2.90−2.93	2.82	5.06	5.85−5.88	158.2−160.2	163.8
K	1.84−1.84	3.04−3.04	2.83	5.37	5.99−5.99	160.7−161.0	180.0
Rb	1.83−1.83	3.07−3.07	2.84	5.44	6.01−6.01	161.6−162.6	180.0
Cs	1.83−1.83	3.07−3.09	2.84	5.59	6.01−6.02	162.4−162.8	179.7

[a]Range represents the shortest and longest, respectively. Notations: U = uranyl; sulf = sulfhydryl. Distances in Angstroms and angles in degrees

Table 7. Selected Geometry Parameters of $A_{10}[(UO_2)_5(S_2)_5(C_2O_4)_5]$ (A = Li, Na, K, Rb, Cs) at the PBE/def-TZVP (COSMO) Level[a]

A	$r(U-O)_U$	$r(U-S)_{per}$	$r(S-S)_{per}$	$r(U-U)_U$	$r(O-O)_{U-U}$	$\angle(OUO)_U$	∠USSU
Li	1.79−1.86	2.79−2.99	2.07−2.11	4.47−4.58	2.79−6.35	175.6−177.3	112.0−116.1
Na	1.81−1.84	2.80−2.97	2.08−2.10	4.53−4.64	2.96−6.28	175.3−178.4	116.6−119.4
K	1.82−1.87	2.82−2.96	2.08−2.09	4.72−4.78	3.21−6.35	176.1−179.1	123.5−124.5
Rb	1.80−1.85	2.83−2.96	2.08−2.09	4.80−4.89	3.37−6.34	176.1−179.3	126.0−128.5
Cs	1.81−1.87	2.84−3.26	2.07−2.12	4.79−5.29	3.30−6.50	173.3−179.0	120.0−146.1

[a]Range represents the shortest and longest, respectively. Notations: U = uranyl; per = persulfide. Distances in Angstroms and angles in degrees

119°. These are smaller than the U−(O_2)−U dihedral angles of 135−140° of the related pentauranyl peroxide cluster.[31]

For the clusters considered, the distances between O atoms belonging to adjacent uranyl ions correlate with the U−(S_2)−U dihedral angle. Their separation is longer in clusters with a U−(S_2)−U dihedral angle of about 180°. The bent dihedral angles in $Na_6[(UO_2)_2(S_2)(O_2)_4]$, $Na_6[(UO_2)_2(S_2)(C_2O_4)_4]$, and $Na_{10}[(UO_2)_5(S_2)_5(C_2O_4)_5]$ are a consequence of the bridging persulfide groups, which ensure a maximum Coulombic attraction between the O atoms of the uranyl ions and the counterion. In $Na_6[(UO_2)_2(SH)_2(O_2)_4]$ and $Na_6[(UO_2)_2(SH)_2(C_2O_4)_4]$, the SH groups do not favor bending as there is no interaction with uranyl.

Insights into the origin of the U−(S_2)−U interaction were obtained through an electronic structure analysis of $Na_6[(UO_2)_2(S_2)(O_2)_4]$ and comparison to $Na_6[(UO_2)_2(O_2)(O_2)_4]$.[31] Selected molecular orbitals (Figure 4) reveal partially delocalized molecular orbitals extending between the U(VI) cations and the bridging persulfide group. A similar bonding orbital exists along the U−$O_{peroxide}$ bond of the diuranyl peroxide cluster.[31] The U−$S_{persulfide}$ bonding orbital is a combination of the persulfide S3p orbitals and minor contributions from the U5f, U6p, and U6d orbitals. In the analogous sulfhydryl cluster, $Na_6[(UO_2)_2(SH)_2(O_2)_4]$, there is no bonding orbital along the U−$S_{sulfhydryl}$ link (Figure 5) due to the lack of a sulfhydryl 3p orbital of the right symmetry to combine with the appropriate uranium orbitals. The molecular orbitals on the SH−SH moieties are localized, and there is no interaction between them. The remaining orbitals in the HOMO−LUMO region correspond to sigma bonding and antibonding orbitals along the O−O bond of the terminal peroxide group. These orbitals are similar in the persulfide and sulfhydryl clusters, in contrast with the diuranyl peroxide case in which the remaining orbitals in the HOMO−LUMO region in the peroxide and hydroxyl clusters are mainly localized on the uranyl moieties.[31] The wave functions of $Na_6[(UO_2)_2(S_2)(O_2)_4]$ and $Na_6[(UO_2)_2(SH)_2(O_2)_4]$ are largely dominated by a single electronic configuration with a weighting of 0.92 and

dx.doi.org/10.1021/ic3008574 | Inorg. Chem. 2012, 51, 7801−7809

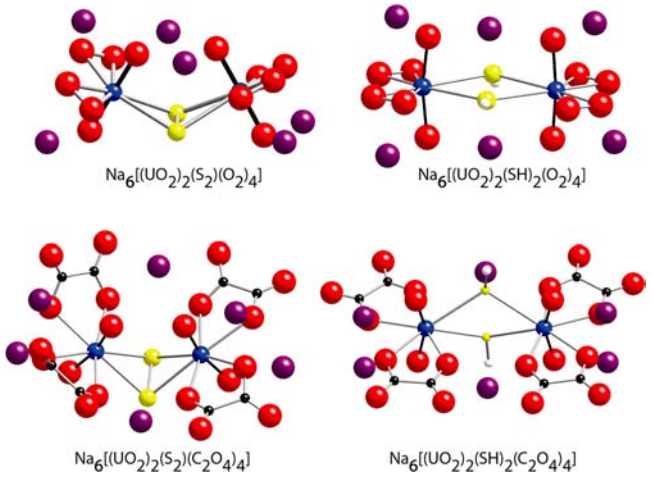

Figure 2. Optimized molecular structures of model clusters at the PBE/def-TZVP (COSMO) level: U, blue; Na, gray; S, yellow; K, dark yellow; O, red; H, white.

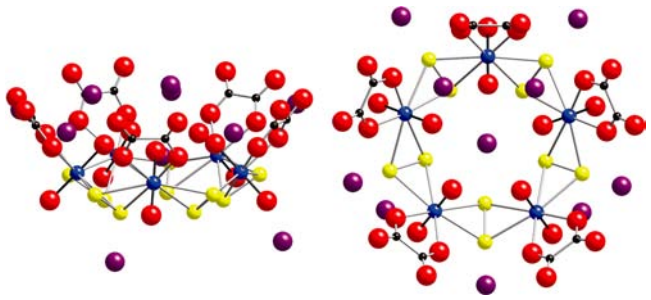

Figure 3. Optimized molecular structures of $K_{10}[(UO_2)_5(S_2)_5(C_2O_4)_5]$ at the PBE/def-TZVP (COSMO) level: U, blue; Na, gray; S, yellow; K, purple; O, red.

0.87, respectively, as would be expected for a closed-shell singlet molecules.

Our calculations reveal that the difference in the U−$S_{persulfide}$ and U−$S_{disulfhydryl}$ bonds favors a bent U−(S_2)−U angle and a planar U−$(SH)_2$−U angle. A stable minimum structure for $Na_6[(UO_2)_2(S_2)(O_2)_4]$ was only obtained upon inclusion of counterions to balance charge, indicating the significant role of the counterions in determining the structure of the cluster. Similarly, for $[(UO_2)_2(O_2)(O_2)_4]^{6-}$, the U−$(O_2)$−U dihedral angle is only bent where the charge of the cluster was balanced by counterions.[31] The interaction of the counterion with the uranyl oxygen atoms makes the uranium atoms more available for interaction with the equatorial sulfur atoms. In the persulfide-bridged cluster a U−$S_{persulfide}$ bond forms, promoting a bent U−(S_2)−U dihedral angle, whereas in the sulfhydryl-bridged cluster a U−$S_{sulfhydryl}$ bond is absent and the S atoms of the sulfhydryl groups are polarized by the presence of H atoms. The average Mulliken atomic charges for U and S are +2.00 and −0.49 in $Na_6[(UO_2)_2(S_2)(O_2)_4]$ and +1.95 and −0.59 in $Na_6[(UO_2)_2(SH)_2(O_2)_4]$, respectively, indicating the S atoms of the sulfhydryl group are more ionic.

Further insight into the U−$S_{persulfide}$ bonding interaction was obtained through an energy decomposition analysis (EDA) for $Na_6[(UO_2)_2(S_2)(O_2)_4]$ (Table 8). The instaneous interaction $\Delta E_{interaction}$ term decomposes into three main components, where the ratio of the electrostatic and orbital interactions, $\Delta E_{elstat}/\Delta E_{orb}$, is used as a description of a bond's covalent and electrostatic character.[74−78] The EDA indicated the electrostatic interaction between the uranyl moieties and persulfide group largely outweighs the orbital interaction (Table 8). On the basis of the $\Delta E_{elstat}/\Delta E_{orb}$ ratio, the U−(S_2)−U interaction is predicted to be more than 75% ionic. A similar EDA on $Na_6[(UO_2)_2(O_2)(O_2)_4]$ predicts the U−(O_2)−U interaction to also be largely ionic (77%),[31] consistent with the comparable molecular orbitals of a localized interaction along the uranyl−persulfide/peroxide bond seen for both systems. Furthermore, the bond dissociation energy indicates considerable stability between uranyl and bridging persulfides. The Voronoi and Hirshfeld atomic charges indicate a positive charge on uranium and an accumulation of negative charge on sulfur of the persulfide bridge (Table 8).

The significance of counterions in producing stable minimum structures as well as bent U−(S_2)−U angles prompted interest in the effect of counterion on the U−(S_2)−U dihedral angle. Geometry optimizations were performed for each cluster under study using A = Li, K, Rb, or Cs as counterions. Selected geometry parameters are reported in Tables 3−7.

In $A_6[(UO_2)_2(S_2)(O_2)_4]$ (Table 3), the U−(S_2)−U dihedral angle decreases with counterion size, from 131° for A = Li to 127° for A = Cs. This trend contrasts with the steady increase in U−(O_2)−U dihedral angle of the peroxo bridge from 140° for A = Li to 164° for A = Cs.[31] For each corresponding cluster and counterion, the U−(S_2)−U dihedral angle is smaller than the analogous U−(O_2)−U dihedral angle (Figure 6). As the size of the counterion is increased, the variation of the U−(S_2)−U dihedral angle is a mere 4°, whereas that of the U−(O_2)−U dihedral angle is 24°.[31]

The optimized geometries for the $A_6[(UO_2)_2(SH)_2(O_2)_4]$ clusters with different counterions (Table 4) indicate that irrespective of the counterion, the U−$(SH)_2$−U dihedral angles are ∼180°, as found for the U−$(OH)_2$−U dihedral angles of

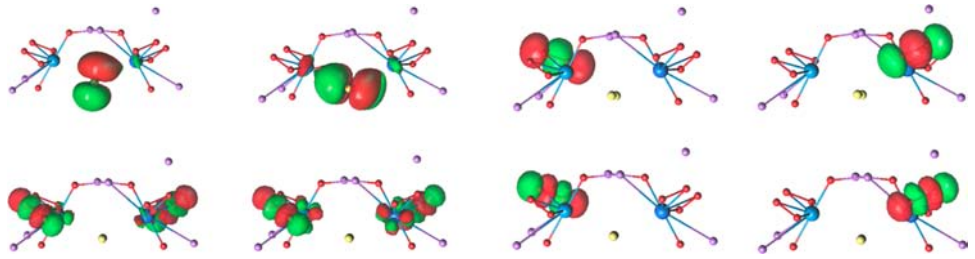

Figure 4. Selected orbitals in $Na_6[(UO_2)_2(S_2)(O_2)_4]$. Two upper left orbitals show interaction between uranyl and the persulfide unit. Remaining orbitals are entirely based on the uranyl peroxo group: U, blue; S, yellow; Na, purple; O, red. Lines show the shortest distance between selected atoms and do not necessarily represent bonds.

dx.doi.org/10.1021/ic3008574 | *Inorg. Chem.* 2012, 51, 7801−7809

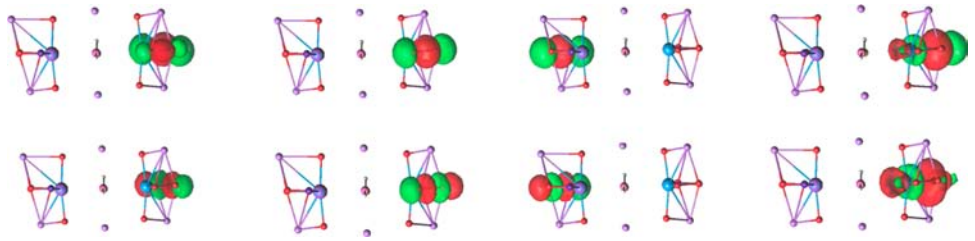

Figure 5. Selected orbitals in $Na_6[(UO_2)_2(SH)_2(O_2)_4]$. Orbitals show no interaction between uranyl and the disulfhydryl unit and are localized on the uranyl peroxo group: U, blue; S, yellow; Na, purple; O, red; H, white. Lines show the shortest distance between selected atoms and do not necessarily represent bonds.

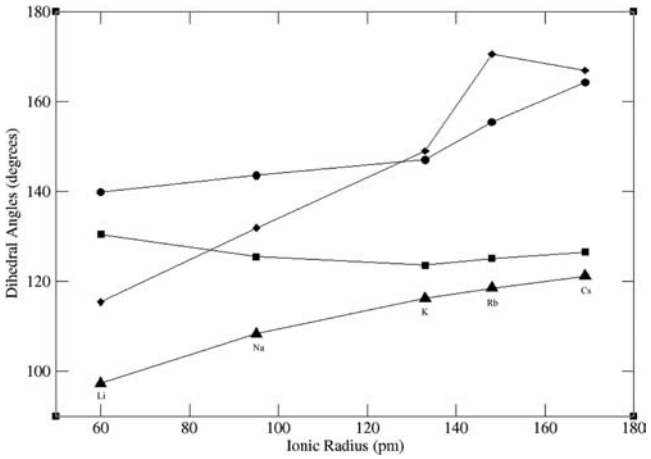

Figure 6. Persulfide (U−S_2−U) and peroxide (U−O_2−U)[31] dihedral angles as a function of counterion ionic radius in $A_6[(UO_2)_2(S_2)(O_2)_4]$ (squares), $A_6[(UO_2)_2(O_2)(O_2)_4]$ (circles), $A_6[(UO_2)_2(S_2)(C_2O_4)_4]$ (triangles), and $A_6[(UO_2)_2(O_2)(C_2O_4)_4]$ (diamonds) (A = Li, Na, K, Rb, Cs).

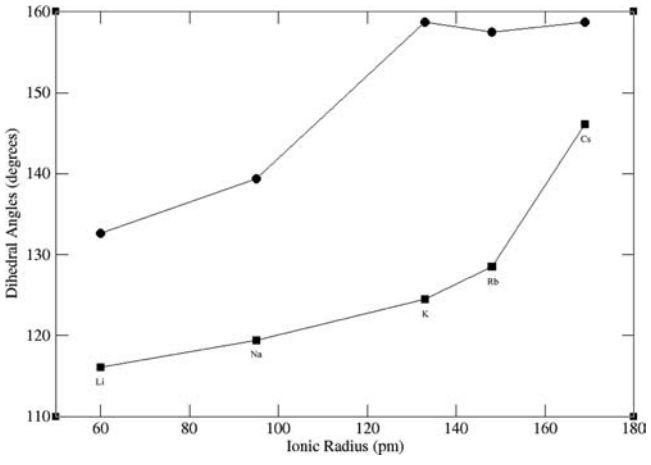

Figure 7. Persulfide (U−S_2−U) and peroxide (U−O_2−U)[31] dihedral angles as a function of counterion ionic radius in $A_{10}[(UO_2)_5(S_2)_5(C_2O_4)_5]$ (squares) and $A_{10}[(UO_2)_5(O_2)_5(C_2O_4)_5]$ (circles) (A = Li, Na, K, Rb, Cs).

the hydroxo-bridged clusters, except for A = K with a dihedral of 157°.[31]

CASSCF/CASPT2 calculations performed for $A_6[(UO_2)_2(S_2)(O_2)_4]$ and $A_6[(UO_2)_2(SH)_2(O_2)_4]$ (A = Li, K, Rb, Cs) provide insight into the electronic structure of the U−S_2−U and U−$(SH)_2$−U interactions. These revealed essentially the same molecular orbital picture irrespective of counterion, and selected molecular orbitals responsible for bonding are provided as Supporting Information.

Table 8. Energy Decomposition Analysis of the U−S_2−U Bond in $Na_6[(UO_2)_2(S_2)(O_2)_4]$ at the ZORA-PBE/def-TZVP Level[a]

	$Na_6[(UO_2)_2(S_2)(O_2)_4]$
ΔE_{orb}	−144.0
ΔE_{elstat}	−492.9
ΔE_{Pauli}	206.8
ΔE_{BDE}	−430.1
% I.C.	77.4
	atomic charge (electron)
Voronoi (U)	0.41
Voronoi (S)	−0.15
Hirshfeld (U)	0.46
Hirshfeld (S)	−0.13

[a]% I.C. = percentage ionic character. Energies in kcal/mol

The influence of terminal groups on structure was investigated by replacing the bidentate peroxo with oxalate ligands. Geometry optimizations of the $A_6[(UO_2)_2(S_2)(C_2O_4)_4]$ clusters (Table 4) resulted in structures comparable with the peroxide-terminated clusters, with the exception of the uranyl ion bond angles for A = Li and Na that became more bent than expected. The U−(S_2)−U dihedral angle varies from 97° for A = Li to 121° for A = Cs, which is the same trend found for the U−(O_2)−U dihedral angles, which increased from 115° for A = Li to 167° for A = Cs.[31] The U−(S_2)−U dihedral angle is smaller than the analgous U−(O_2)−U dihedral angle for each corresponding cluster and counterion (Figure 6). As counterion size is increased, the U−(S_2)−U and U−(O_2)−U dihedral angles vary by 24° and 52°, respectively.

Geometry parameters of the sulfhydryl-bridged cluster $A_6[(UO_2)_2(SH)_2(C_2O_4)_4]$ (Table 6) show that although the uranyl ion geometry remains essentially constant as the counterion is changed, the uranyl ion bond angle is significantly bent, similar to results for the analogous diuranyl peroxide clusters.[31] Furthermore, in some cases the two SH groups do not remain in the equatorial plane of a hexagonal bipyramid about the uranyl ion, as shown in the case of $Na_6[(UO_2)_2(SH)_2(C_2O_4)_4]$ in Figure 2. The U−$(SH)_2$−U dihedral angles are ∼180° for A = K, Rb, and Cs and 142° and 164° for A = Li and Na, respectively, with a similar departure from planarity found for the U−$(OH)_2$−U dihedral angle for A = Li of 150°.[31]

Geometry parameters for the $A_{10}[(UO_2)_5(S_2)_5(C_2O_4)_5]$ clusters (Table 7, Figure 3) include calculated uranyl ion bond lengths and angles that are consistent with experimentally derived values[17] and those in the analogous pentauranyl

dx.doi.org/10.1021/ic3008574 | Inorg. Chem. 2012, 51, 7801−7809

peroxide cluster.[31] Increasing counterion size flattens the overall structure from a U−(S_2)−U dihedral angle of 112−116° for A = Li to 120−146° for A = Cs. A similar trend was found for the U−(O_2)−U dihedral angles of the pentauranyl peroxide clusters, which varies from 129−133° for A = Li to 157−158° for A = Cs.[31] The persulfide and peroxide[31] dihedral angles as a function of the ionic radius of the counterion[79] (Figure 7) follow similar trends, although the U−(S_2)−U dihedral angles are smaller than the analgous U−(O_2)−U dihedral angles. The U−(S_2)−U and U−(O_2)−U dihedral angles vary by margins of 34° and 29°, respectively, with counterion size.

4. DISCUSSION AND CONCLUSIONS

Our synthesis of crystals of $Na_4[(UO_2)(S_2)_3](CH_3OH)_8$ using standard inert-atmosphere methods demonstrate that the $[(UO_2)(S_2)_3]^{4-}$ unit can be created at room temperature under manageable experimental conditions. Methods are currently being developed for the synthesis of compounds containing uranyl ions that are bridged through persulfide ligands, which is an essential step toward forming cage clusters.

All of our calculations support the conclusion that bidentate persulfide bridges between uranyl ions include a partial covalent interaction that favors a bent U−(S_2)−U dihedral angle. As such, assembly of multiple uranyl polyhedra through persulfide bridges may result in structures with curvature and potential nanoscale clusters as observed in the uranyl peroxo system. However, for a given counterion, the calculated U−(S_2)−U dihedral angles are invariably smaller than those of the corresponding cluster with peroxo bridges, a finding that may have important implications for nanoscale cluster formation.

Consider the case of linkages of $[(UO_2)(S_2)_3]^{4-}$ species into cage clusters through the sharing of bidentate persulfide between uranyl ions. A major constraint is that the three persulfide groups of a given uranyl ion are in a coplanar arrangement at the edges of a hexagonal bipyramid. As such, linkage of $[(UO_2)(S_2)_3]^{4-}$ polyhedra through persulfide groups with U−(S_2)−U dihedral angles of 180° could only give a flat chain or a two-dimensional sheet. A bent U−(S_2)−U dihedral angle gives curvature, and if a cage cluster is assembled, it is the dihedral angle that dictates how many polyhedra are needed to close the cluster. For example, the lowest number of vertices in a fullerene topology is 20, as observed for U_{20} with peroxide bridges,[16] and the required dihedral angle is 140°. This is therefore the average U−(S_2)−U dihedral angle that is needed to form a cluster with 20 $[(UO_2)(S_2)_3]^{4-}$ polyhedra and a fullerene topology. Our calculations indicate that optimal U−(S_2)−U dihedral angles in our model clusters range from 97° to 130.5° and therefore suggest that it is unlikely that such a cluster can be synthesized.

Again considering specifically the $[(UO_2)(S_2)_3]^{4-}$ species, we do not expect it to assemble into cage clusters with fullerene topologies containing more than 20 vertices as this would require even more opened U−(S_2)−U dihedral angles than one with 20 vertices. However, while it is presumably essential to maintain some persulfide bridges to encourage curvature, it may be possible to bridge between uranyl ions through two SH groups (as shown by our calculations) or through oxalate or other groups. These bridges are typically nearly flat. This approach was used in the case of uranyl peroxo polyhedra and resulted in a wide range of topologies. Linkage of the species $[(UO_2)(S_2)(SH)_4]^{4-}$ through U−(S_2)−U and U−$(SH)_2$−U bridges could give an average dihedral angle of ∼150−160°, which is consistent with formation of clusters such as U_{60} with U−(O_2)−U and U−$(OH)_2$−U bridges with an average dihedral angle of 155°.[16]

■ ASSOCIATED CONTENT

Supporting Information

Coordinates of the optimized structures, molecular orbital diagrams, crystallographic information file (CIF), and Raman, IR and UV−vis spectra for $Na_4[(UO_2)(S_2)_3](CH_3OH)_8$. This material is available free of charge via the Internet at http://pubs.acs.org.

■ AUTHOR INFORMATION

Corresponding Author

*E-mail: pburns@nd.edu (P.C.B.); gagliard@umn.edu (L.G.).

Notes

The authors declare no competing financial interest.

■ ACKNOWLEDGMENTS

This research was supported by the Materials Science of Actinides Center, an Energy Frontier Research Center funded by the U.S. Department of Energy, Office of Science, Office of Basic Energy Sciences under Award Number DE-SC0001089.

■ REFERENCES

(1) Pope, M. T.; Muller, A. *Angew. Chem., Int. Ed. Engl.* **1991**, *30*, 34.
(2) Muller, A.; Peters, F.; Pope, M. T.; Gatteschi, D. *Chem. Rev.* **1998**, *98*, 239.
(3) Liu, T. B.; Imber, B.; Diemann, E.; Liu, G.; Cokleski, K.; Li, H. L.; Chen, Z. Q.; Muller, A. *J. Am. Chem. Soc.* **2006**, *128*, 15914.
(4) Long, D. L.; Tsunashima, R.; Cronin, L. *Angew. Chem., Int. Ed.* **2010**, *49*, 1736.
(5) Miras, H. N.; Cooper, G. J. T.; Long, D. L.; Bogge, H.; Muller, A.; Streb, C.; Cronin, L. *Science* **2010**, *327*, 72.
(6) Muller, A.; Roy, S. *Coord. Chem. Rev.* **2003**, *245*, 153.
(7) Morss, L. R.; Edelstein, N. M.; Fuger, J.; Katz, J. J. *The Chemistry of the Actinide and Transactinide Elements*; Springer: Dordrecht, 2006.
(8) Nocton, G.; Burdet, F.; Pecaut, J.; Mazzanti, M. *Angew. Chem., Int. Ed.* **2007**, *46*, 7574.
(9) Nocton, G.; Pecaut, J.; Filinchuk, Y.; Mazzanti, M. *Chem. Commun.* **2010**, *46*, 2757.
(10) Nocton, G.; Pecaut, J.; Mazzanti, M. *Angew. Chem., Int. Ed.* **2008**, *47*, 3040.
(11) Biswas, B.; Mougel, V.; Pecaut, J.; Mazzanti, M. *Angew. Chem., Int. Ed.* **2011**, *50*, 5744.
(12) Duval, P. B.; Burns, C. J.; Clark, D. L.; Morris, D. E.; Scott, B. L.; Thompson, J. D.; Werkema, E. L.; Jia, L.; Andersen, R. A. *Angew. Chem., Int. Ed.* **2001**, *40*, 3358.
(13) Soderholm, L.; Almond, P. M.; Skanthakumar, S.; Wilson, R. E.; Burns, P. C. *Angew. Chem., Int. Ed.* **2008**, *47*, 298.
(14) Burns, P. C.; Kubatko, K. A.; Sigmon, G.; Fryer, B. J.; Gagnon, J. E.; Antonio, M. R.; Soderholm, L. *Angew. Chem., Int. Ed.* **2005**, *44*, 2135.
(15) Forbes, T. Z.; McAlpin, J. G.; Murphy, R.; Burns, P. C. *Angew. Chem., Int. Ed.* **2008**, *47*, 2824.
(16) Sigmon, G. E.; Ling, J.; Unruh, D. K.; Moore-Shay, L.; Ward, M.; Weaver, B.; Burns, P. C. *J. Am. Chem. Soc.* **2009**, *131*, 16648.
(17) Sigmon, G. E.; Unruh, D. K.; Ling, J.; Weaver, B.; Ward, M.; Pressprich, L.; Simonetti, A.; Burns, P. C. *Angew. Chem., Int. Ed.* **2009**, *48*, 2737.
(18) Sigmon, G. E.; Weaver, B.; Kubatko, K. A.; Burns, P. C. *Inorg. Chem.* **2009**, *48*, 10907.
(19) Ling, J.; Qiu, J.; Sigmon, G. E.; Ward, M.; Szymanowski, J. E. S.; Burns, P. C. *J. Am. Chem. Soc.* **2010**, *132*, 13395.
(20) Ling, J.; Wallace, C. M.; Szymanowski, J. E. S.; Burns, P. C. *Angew. Chem., Int. Ed.* **2010**, *49*, 7271.

(21) Unruh, D. K.; Burtner, A.; Pressprich, L.; Sigmon, G. E.; Burns, P. C. *Dalton Trans.* **2010**, *39*, 5807.
(22) Ling, J.; Qiu, J.; Szymanowski, J. E. S.; Burns, P. C. *Chem.—Eur. J.* **2011**, *17*, 2571.
(23) Nyman, M.; Rodriguez, M. A.; Alam, T. M. *Eur. J. Inorg. Chem.* **2011**, 2197.
(24) Sigmon, G. E.; Burns, P. C. *J. Am. Chem. Soc.* **2011**, *133*, 9137.
(25) Unruh, D. K.; Ling, J.; Qiu, J.; Pressprich, L.; Baranay, M.; Ward, M.; Burns, P. C. *Inorg. Chem.* **2011**, *50*, 5509.
(26) Ling, J.; Qiu, J.; Burns, P. C. *Inorg. Chem.* **2012**, *51*.
(27) Qiu, J.; Ling, J.; Sui, A.; Szymanowski, J. E. S.; Simonetti, A.; Burns, P. C. *J. Am. Chem. Soc.* **2012**, *134*.
(28) Armstrong, C. R.; Nyman, M.; Shvareva, T.; Sigmon, G. E.; Burns, P. C.; Navrotsky, A. *Proc. Natl. Acad. Sci. U.S.A.* **2012**, *109*, 1874.
(29) Burns, P. C.; Ewing, R. C.; Navrotsky, A. *Science* **2012**, *335*, 1184.
(30) Miro, P.; Pierrefixe, S.; Gicquel, M.; Gil, A.; Bo, C. *J. Am. Chem. Soc.* **2010**, *132*, 17787.
(31) Vlaisavljevich, B.; Gagliardi, L.; Burns, P. C. *J. Am. Chem. Soc.* **2010**, *132*, 14503.
(32) Sutorik, A. C.; Kanatzidis, M. G. *Polyhedron* **1997**, *16*, 3921.
(33) Perry, D. L.; Zalkin, A.; Ruben, H.; Templeton, D. H. *Inorg. Chem.* **1982**, *21*, 237.
(34) Repichet, S.; Zwick, A.; Vendier, L.; Le Roux, C.; Dubac, J. *Tetrahedron Lett.* **2002**, *43*, 993.
(35) *Bruker*; Bruker AXS, Inc.: Madison, WI, USA, 2007.
(36) Sheldrick, G. M. *Acta Crystallogr., Sect. A* **2008**, *64*, 112.
(37) Hohenberg, P.; Kohn, W. *Phys. Rev. B* **1964**, *136*, B864.
(38) Kohn, W.; Sham, L. J. *Phys. Rev.* **1965**, *140*, 1133.
(39) Roos, B. O.; Taylor, P. R.; Siegbahn, P. E. M. *Chem. Phys.* **1980**, *48*, 157.
(40) Andersson, K.; Malmqvist, P. A.; Roos, B. O. *J. Chem. Phys.* **1992**, *96*, 1218.
(41) Weigend, F.; Haser, M.; Patzelt, H.; Ahlrichs, R. *Chem. Phys. Lett.* **1998**, *294*, 143.
(42) Perdew, J. P.; Burke, K.; Ernzerhof, M. *Phys. Rev. Lett.* **1996**, *77*, 3865.
(43) Schafer, A.; Huber, C.; Ahlrichs, R. *J. Chem. Phys.* **1994**, *100*, 5829.
(44) Eichkorn, K.; Weigend, F.; Treutler, O.; Ahlrichs, R. *Theor. Chem. Acc.* **1997**, *97*, 119.
(45) Cao, X. Y.; Dolg, M. *J. Chem. Phys.* **2001**, *115*, 7348.
(46) Klamt, A.; Schuurmann, G. *J. Chem. So., Perkin Trans. 2* **1993**, 799.
(47) Grant, D. J.; Stewart, T. J.; Bau, R.; Miller, K. A.; Mason, S. A.; Gutmann, M.; McIntyre, G. J.; Gagliardi, L.; Evans, W. J. *Inorg. Chem.* **2012**, *51*, 3613.
(48) Ahlrichs, R.; Bar, M.; Haser, M.; Horn, H.; Kolmel, C. *Chem. Phys. Lett.* **1989**, *162*, 165.
(49) van Lenthe, E.; Ehlers, A.; Baerends, E. J. *J. Chem. Phys.* **1999**, *110*, 8943.
(50) Velde, G. T.; Bickelhaupt, F. M.; Baerends, E. J.; Guerra, C. F.; Van Gisbergen, S. J. A.; Snijders, J. G.; Ziegler, T. *J. Comput. Chem.* **2001**, *22*, 931.
(51) Morokuma, K. *Acc. Chem. Res.* **1977**, *10*, 294.
(52) Morokuma, K. *J. Chem. Phys.* **1971**, *55*, 1236.
(53) Ziegler, T.; Rauk, A. *Theor. Chim. Acta* **1977**, *46*, 1.
(54) Ziegler, T.; Rauk, A. *Inorg. Chem.* **1979**, *18*, 1558.
(55) Ziegler, T.; Rauk, A. *Inorg. Chem.* **1979**, *18*, 1755.
(56) Roos, B. O.; Lindh, R.; Malmqvist, P. A.; Veryazov, V.; Widmark, P. O. *J. Phys. Chem. A* **2005**, *109*, 6575.
(57) Hess, B. A. *Phys. Rev. A* **1986**, *33*, 3742.
(58) Gagliardi, L.; Roos, B. O. *Chem. Phys. Lett.* **2000**, *331*, 229.
(59) Hagberg, D.; Karlstrom, G.; Roos, B. O.; Gagliardi, L. *J. Am. Chem. Soc.* **2005**, *127*, 14250.
(60) Karlstrom, G.; Lindh, R.; Malmqvist, P. A.; Roos, B. O.; Ryde, U.; Veryazov, V.; Widmark, P. O.; Cossi, M.; Schimmelpfennig, B.; Neogrady, P.; Seijo, L. *Comput. Mater. Sci.* **2003**, *28*, 222.
(61) Aquilante, F.; Gagliardi, L.; Pedersen, T. B.; Lindh, R. *J. Chem. Phys.* **2009**, *130*, 154107.
(62) Aquilante, F.; Pedersen, T. B.; Lindh, R.; Roos, B. O.; De Meras, A. S.; Koch, H. *J. Chem. Phys.* **2008**, *129*, 024113.
(63) Aquilante, F.; Malmqvist, P. A.; Pedersen, T. B.; Ghosh, A.; Roos, B. O. *J. Chem. Theory Comput.* **2008**, *4*, 694.
(64) Aquilante, F.; Pedersen, T. B.; Lindh, R. *J. Chem. Phys.* **2007**, *126*, 194106.
(65) Gagliardi, L.; Roos, B. O. *Chem. Soc. Rev.* **2007**, *36*, 893.
(66) Gagliardi, L. *J. Am. Chem. Soc.* **2003**, *125*, 7504.
(67) La Macchia, G.; Brynda, M.; Gagliardi, L. *Angew. Chem., Int. Ed.* **2006**, *45*, 6210.
(68) Gagliardi, L.; Heaven, M. C.; Krogh, J. W.; Roos, B. O. *J. Am. Chem. Soc.* **2005**, *127*, 86.
(69) Roos, B. O.; Widmark, P. O.; Gagliardi, L. *Faraday Discuss.* **2003**, *124*, 57.
(70) Burns, P. C. *Can. Mineral.* **2005**, *43*, 1839.
(71) Cejka, J. *Infrared spectroscopy and thermal analysis of the uranyl minerals*; Mineralogical Society of America: Washington D.C., 1999; Vol. *38*.
(72) Turcotte, S. B.; Benner, R. E.; Riley, A. M.; Li, J.; Wadsworth, M. E.; Bodily, D. *Appl. Opt.* **1993**, *32*, 935.
(73) Turcotte, S. B.; Benner, R. E.; Riley, A. M.; Li, J.; Wadsworth, M. E.; Bodily, D. M. *J. Electroanal. Chem.* **1993**, *347*, 195.
(74) Diefenbach, A.; Bickelhaupt, F. M.; Frenking, G. *J. Am. Chem. Soc.* **2000**, *122*, 6449.
(75) Uddin, J.; Frenking, G. *J. Am. Chem. Soc.* **2001**, *123*, 1683.
(76) Pandey, K. K.; Lein, M.; Frenking, G. *J. Am. Chem. Soc.* **2003**, *125*, 1660.
(77) Pandey, K. K. *Inorg. Chem.* **2003**, *42*, 6764.
(78) Frenking, G.; Wichmann, K.; Frohlich, N.; Loschen, C.; Lein, M.; Frunzke, J.; Rayon, V. M. *Coord. Chem. Rev.* **2003**, *238*, 55.
(79) Huheey, J. E.; Keiter, E. A.; Keiter, R. L. *Inorganic Chemistry: Principles of Structure and Reactivity*; 4th ed.; Harper Collins: New York, 1993.